https://doi.org/10.5194/hess-2024-25
Preprint. Discussion started: 5 March 2024
© Author(s) 2024. CC BY 4.0 License.

Hydrology and Earth System Sciences
Open Access
EGU
Discussions

Ratio Limits of Water Storage and Outflow in Rainfall-runoff Process

Yulong Zhu[a], Yang Zhou[b], Xiaorong Xu[c], Changqing Meng[d], and Yuankun Wang[e*]

[a]**Yulong Zhu**

School of Water Resources and Hydropower Engineering, North China Electric Power University, Changping Beinong 2# 102206, Beijing, China. Email: zhuyulong@ncepu.edu.cn

[b]**Yang Zhou**

School of Water Resources and Hydropower Engineering, North China Electric Power University, Changping Beinong 2# 102206, Beijing, China. Email: zhouyang@ncepu.edu.cn

[c]**Xiaorong Xu**

School of Water Resources and Hydropower Engineering, North China Electric Power University, Changping Beinong 2# 102206, Beijing, China. Email: xxrong@ncepu.edu.cn

[d]**Changqing Meng**

School of Water Resources and Hydropower Engineering, North China Electric Power University, Changping Beinong 2# 102206, Beijing, China. Email: els_meng@ncepu.edu.cn

[e*]**Yuankun Wang** (Corresponding author)

School of Water Resources and Hydropower Engineering, North China Electric Power University, Changping Beinong 2# 102206, Beijing, China. Email: yuankunw@ncepu.edu.cn

https://doi.org/10.5194/hess-2024-25
Preprint. Discussion started: 5 March 2024
© Author(s) 2024. CC BY 4.0 License.

Hydrology and Earth System Sciences
Open Access
Discussions
EGU

Abstract

Through the numerical simulations of the hydrodynamic model, the water storage and discharge are found to be limited to envelope lines and the discharge/water depth process lines during water rising and falling showed a grid-shaped distribution. Furthermore, if a catchment is regarded as a semi-open water storage system, there is a nonlinear relationship between the inside average water depth and the outlet water depth, namely the water storage ratio curve, which resembles the shape of a "plume". In the case of an open channel without considering spatial variability, the water storage ratio curve is limited to three values (i.e., the upper, the steady, and the lower limit), which are found to be independent of meteorological (rainfall intensity), vegetation (Manning's coefficient), and terrain (slope gradient) conditions. Meteorological, vegetation, and terrain conditions only affect the size of the "plume" without changing its shape. Rainfall, especially weak rain (rainfall intensity is less than 5.0 mm h^{-1}) significantly affects the fluctuations of water storage ratio, which can be divided into three modes, that is Mode I during rainfall beginning stage, Mode II during rainfall duration stage, and Mode III during rainfall end stage. Results indicate that the determination of the nonlinear relationship of the water storage ratio curve under different geographical scenarios will provide new ideas for simulation and early warning of floods.

1. Introduction

Flood disaster is a significant global health and economic threat. Disastrous floods have caused millions of fatalities in the twentieth century and billions of dollars direct economic loss each year (Merkuryeva, et al., 2015; Merz, et al., 2021; Ruidas, et al., 2022). Weather prediction-based distributed hydrological/hydraulic models are considered to be an effective strategy for flood forecasting (Ming, et al., 2020). According to statistics (Lee, et al., 2020), from 2001 to 2018, over 2,900 floods caused over 93,000 deaths and over 490 billion USD in economic damages worldwide. Based on the daily satellite imagery at 250-metre resolution of the 913 large flood events in the same period, a total inundation area of 2.23 million km^2, with 255-290

https://doi.org/10.5194/hess-2024-25
Preprint. Discussion started: 5 March 2024
© Author(s) 2024. CC BY 4.0 License.
Hydrology and Earth System Sciences Discussions

million people were estimated directly affected by floods (Tellman, et al., 2021). With the influence of climate change and extreme El Niño events (Ward, et al., 2014; Cai, et al., 2014), flood events caused by extreme precipitation are occurring frequently in many regions around the world (Kirezci, et al., 2020; Najibi and Devineni, 2018; Almazroui, 2020). From 2020 to 2023, catastrophic floods caused by several extreme rainfall events were reported in Germany (Tradowsky, et al., 2023), China (Hsu, et al., 2021), Italy (Valente, et al., 2023), Japan (Kobayashi, et al., 2023), Pakistan (Nanditha, et al., 2023) and other developed or developing countries and regions, even in some desert areas (e.g., Taklimakan Desert (Li and Yao, 2023) and Atacama Desert (Cabré, et al., 2023)). Research shows that under a high emissions scenario, in latitudes above 40° north, compound flooding could become more than 2.5 times as frequent by 2100 compared to present (Bevacqua, et al., 2020). It means that in future, the fraction of the global population at risk of floods will be growing.

Flood simulation provides an effective means of flood forecasting to reduce property and life losses in flood-threatened areas around the world. A large number of scholars are committed to shortening the simulation time of floods. Accordingly, they have developed many forms of hydrological models (e.g., Stanford Watershed Model IV (SWM) (Crawford and Linsley, 1966), SHE/MIKESHE model (Abbott, et al., 1986), Tank model (Sugawara, 1995), Soil and Water Assessment Tool (SWAT) (Arnold and Williams, 1987), TOPMODEL (Beven and Kirkby, 1979), etc.), hydrodynamic models (the one-dimension(1D) Saint-Venant equation (Köhne, et al., 2011), the two-dimensions (2D) shallow water equations (SWEs) (Camassa, et al., 1994), and the three-dimensions (3D) integrated equations of runoff and seepage (Mori, et al., 2015)), or coupling models of the two (Kim, et al., 2012; Liu, et al., 2019; Hoch, et al., 2019). Particularly, SWEs are the main governing equations for simulating flood. However, flood simulation based on SWEs is a time-consuming process due to its governing equations are a hyperbolic system of first-order nonlinear partial differential equations (PDEs) (Li and Fan, 2017). Therefore, many scholars attempted to improve the

https://doi.org/10.5194/hess-2024-25
Preprint. Discussion started: 5 March 2024
© Author(s) 2024. CC BY 4.0 License.
Hydrology and Earth System Sciences
Open Access
EGU
Discussions

efficiency and accuracy of flood simulation through computer technology (GPU parallel computing (Crossley, et al., 2010) or advanced numerical scheme (Sanders, et al., 2010)). For hydrological studies, the performance of hydrological modeling is usually challenged by model calibration and uncertainty analysis during modeling exercises (Wu, et al., 2021).

Hence, we try to ignore the complex exchange/transfer process of mass and momentum (hydrodynamic models), and also abandon the empirical relationships (hydrological models) between the input (precipitation), the transmission (flow rate) and the output (discharge) in the catchment area. A catchment is regarded as a semi-open water storage system. For the storage system, the complex problem is simplified into three megascopic variables, i.e., inflow, water storage and outflow. If we can give a physical-based relationship between the three, flood forecasting will become much simpler.

2. Methods

An arbitrary catchment (Fig. 1b) could be assumed to be a conceptual water tank (Fig. 1a). In this water tank, according to the law of conservation of mass, the complex confluence process of surface runoff could be neglected and it can be described only by the relationship between input (average rainfall (R) and exfiltration (-I)), storage (characterized by the internal average water depth (H)), and output (average infiltration (I), evaporation (E), and discharge (Q)), which can be expressed as Eq. 1,

$$\underbrace{A \times \frac{dH}{dt}}_{storage} = \underbrace{R \times A}_{rainfall} \mp \underbrace{\boldsymbol{I \times A}}_{\substack{infiltration \\ /exfiltration}} - \underbrace{E \times A}_{\textbf{evaporation}} - \underbrace{\frac{Q}{A} \times A}_{discharge} \tag{1}$$

In this paper, attentions are focused on the surface flow of runoff, so the runoff-atmosphere moisture exchange (evaporation) and runoff-soil moisture exchange (infiltration and/or exfiltration) are non-considered. Zhu et al. (2020) validated the effectiveness of a diffusion wave (DW) approximation of shallow water equations by numerical simulations for simulating ground surface runoff,

$$\frac{\partial h}{\partial t} - \nabla\left(\frac{h^{5/3}}{n_m\sqrt{|S|}}\nabla(h+z)\right) = R \tag{2}$$

To improve the computational efficiency of hydrodynamic model, after strict mathematical derivation according to the basic hydrodynamic equation and the law of conservation of mass, Zhu et al. (2022) proposed a hydrological-hydrodynamic integrated model, i.e., distributed runoff model (DRM) as,

$$\begin{cases} \frac{dH}{dt} = R - q \\ H = \eta h = \eta \left(\frac{n_m}{\sqrt{S}}\right)^{0.6} q^{0.6} \left(\frac{A}{B}\right)^{0.6} \end{cases} \quad (3)$$

where, R indicates rainfall intensity (m s^{-1}); q is conceptual outflow (m s^{-1}), q=Q/A (m s^{-1}); n_m is Manning's coefficient (s m$^{-1/3}$); S is the slope gradient; η is the water storage ratio; A is catchment area (m^2) and B is the outlet width (m).

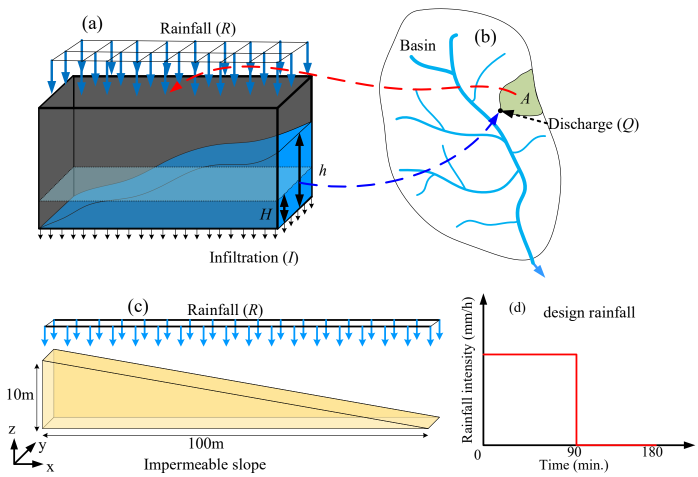

Fig. 1. Conceptual schematic of the DRM and numerical model. (a) conceptual water tank; (b) conceptual catchment; (c) impermeable conceptual slope model; (d) designed rainfall.

3. Limits and "plume" shape of water storage ratio curve

The conceptual hydrological model takes the inside average water depth (H) in the catchment area as the independent variable (Eq. 1). However, the hydrodynamic equations take the water depth at any outlet (h) as an independent variable (Eq. 2). If a relationship between the inside average water depth (H) and outlet water depth (h) can be established, then this relationship will have both hydrodynamic and hydrological characteristics. Therefore, to find the H-h relationship, an impermeable conceptual slope model was built as shown in Fig. 1c and numerical simulations are performed using diffusion wave (DW) approximation (Eq. 2)

https://doi.org/10.5194/hess-2024-25
Preprint. Discussion started: 5 March 2024
© Author(s) 2024. CC BY 4.0 License.

of shallow water equations (SWEs). The water storage ratio is defined as the inside average water depth (H) divided by the outlet water depth (h). Firstly, the numerical simulations are performed under a designed rainfall condition, i.e., rainfall intensity is 10 mm h^{-1} and rainfall duration are 90 minutes with the total time of 180 minutes as shown in Fig. 1d. From the time-dependent water storage ratio (H/h) under different catchment area (Fig. 2a), it can be seen that the continuous rainfall will cause the water storage ratio (H/h) to gradually decrease from the initial value 1.0 (upper limit) to a stable value, which is approximately 0.625 (steady limit). When the rainfall ends, the value of the water storage ratio (H/h) decreases first and then increases, showing a U-shaped curve with a lower limit, which is approximately 0.4125. Afterward, the water storage ratio curves under ten kinds of catchment area (Fig. 2b), three kinds of Manning's coefficient (Fig. 2c), four kinds of slope gradient (Fig. 2d), and four kinds of rainfall intensity (Fig. 2e) conditions are obtained from parametric analyses and summarized in Fig. 2f.

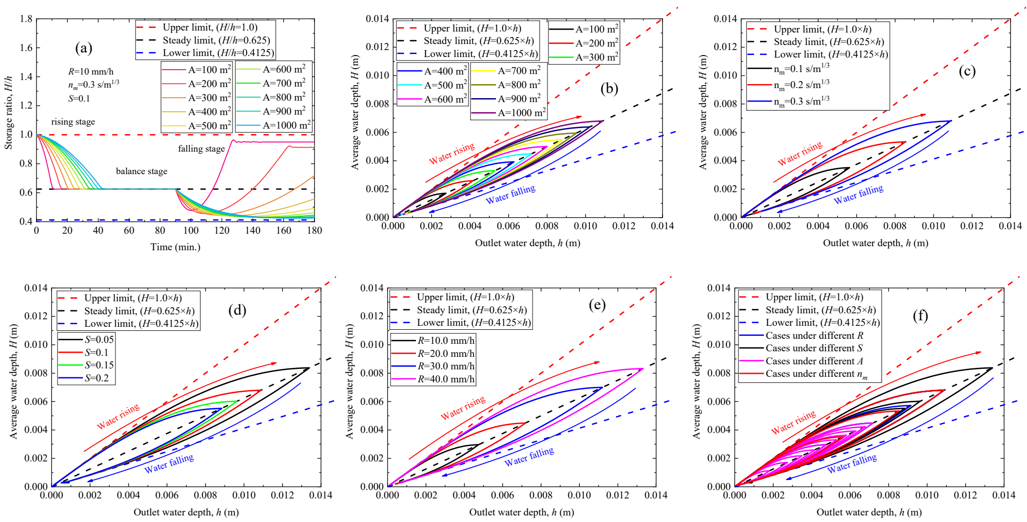

Fig. 2. Water storage ratio curves. (a) Time-dependent water storage ratio under different catchment area with 10 mm h^{-1}. Water storage ratio curves under different (b) catchment area (A); (c) Manning's coefficient (n_m); (d) slope gradient (S); and (e) rainfall intensity rainfall intensity (R). (f) Three limit lines envelop all water storage ratio curves, i.e., Upper limit (H/h=1.0), Steady limit(H/h=0.625), and Lower

https://doi.org/10.5194/hess-2024-25
Preprint. Discussion started: 5 March 2024
© Author(s) 2024. CC BY 4.0 License.
Hydrology and Earth System Sciences
Discussions

limit(H/h=0.4125).

Finally, it is found that water storage ratio curves resemble a shape of "plume". Higher water storage ratio (H/h) for the water-rising limb than for the water-falling limb at the same outlet water depth. Furthermore, in the case of an open channel without considering spatial variability, there are three limits (the upper, the steady, and the lower limit) of the water storage ratio curves, which are found to be independent of meteorological (rainfall intensity), vegetation (Manning's coefficient), and terrain (slope gradient) conditions. Meteorological, vegetation, and terrain conditions only affect the size of the "plume" without changing its shape that is anchored by three limits. This means that the three limits and the water storage ratio curves provide a key to establish a relationship between the hydrodynamic models and the hydrological models.

4. Grid-shaped cross distribution of discharge/water depth process lines during water rising and falling

To obtain further insights into the causes for the formation of the water-rising limb and the water-falling limb of the water storage ratio curve. The ratio of discharge (i.e., the ratio of the total outflows (Q_{out}) to the total inflows (Q_{in}), and the water depth (h) along the slope are discussed in Fig. 3a and Fig. 3b, respectively. Results indicate that there is an envelope line that controls the distribution of the discharge and water depth along the slope, respectively. The discharge envelope line is a straight line with a slope of 1.0 (Fig. 3a), while the water depth envelope line is a nonlinear curve controlled by power function ($h=kx^a$) (Fig. 3b). It means that if the duration of rainfall with a constant intensity is long enough, the catchment system will eventually reach an equilibrium state between inflow and outflow.

On the other hand, the process lines of discharge and water depth during water rising and falling present a grid-shaped cross distribution (Fig. 3a and Fig. 3b). Similarly, from the view of the gradient of the discharge and water depth process lines during water rising and falling, the discharge gradient curves (Fig. 3c) and the water depth gradient curves (Fig. 3d) also present a grid-shaped cross distribution during water

https://doi.org/10.5194/hess-2024-25
Preprint. Discussion started: 5 March 2024
© Author(s) 2024. CC BY 4.0 License.
Hydrology and Earth System Sciences
Open Access
Discussions

rising and falling, which might be the cause of the looped rating curve (Fig. 3e), i.e., higher discharges for the rising limb (Q_u) than for the recession limb (Q_f) at the same stage (Petersen-Øverleir, 2006). After fitting the value of parameter k and a under different rainfall intensity (R), Manning's coefficient (n_m), and slope gradient (S) conditions (Fig. 3f), it is found that the parameter a is a constant, while the change of parameter k is positively correlated with the change of rainfall intensity (R) and Manning's coefficient (n_m), but negatively correlated with the change of slope gradient (S).

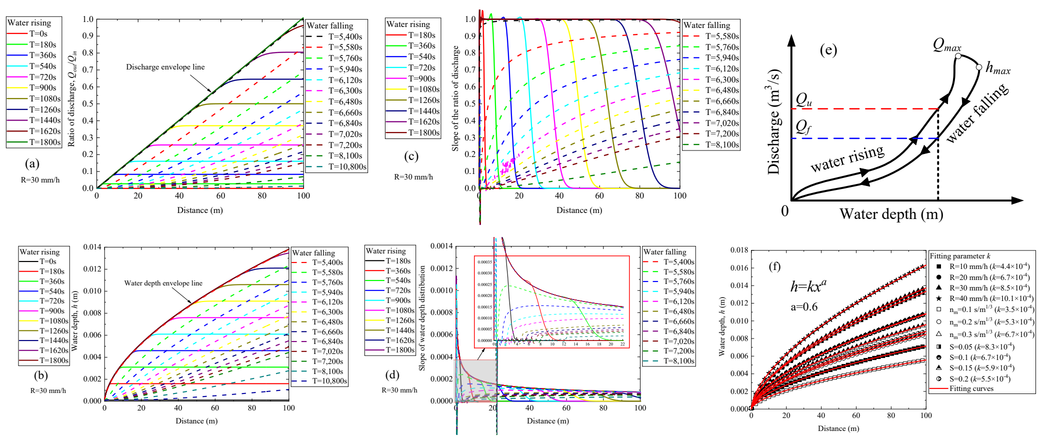

Fig. 3. Discharge/water depth process lines during water rising and falling. (a) discharge process lines during water rising and falling; (b) gradient lines of discharge process line during water rising and falling; (c) schematic diagram of looped rating curve; (d) water depth process lines during water rising and falling; (e) gradient lines of water depth process lines during water rising and falling; (f) change of water depth envelope line under different rainfall intensity (R), Manning's coefficient (n_m), and slope gradient (S).

Based on the water storage ratio curve, a hydrological-hydrodynamic integrated model, namely the Distributed Runoff Model (DRM), is established with the governing equations in Eq. 3. To check the effectiveness and applicability of DRM, the comparative analysis of the numerical results obtained from the DRM and the DW model is implemented. We found that the DRM quickly reproduces the calculation results of the time-consuming DW model under different rainfall intensity (Fig. 4a and Fig. 4b), different Manning's coefficient and different slope gradient (Fig. 4c and Fig. 4d). meaning that the water storage ratio curve will

https://doi.org/10.5194/hess-2024-25
Preprint. Discussion started: 5 March 2024
© Author(s) 2024. CC BY 4.0 License.
Hydrology and Earth System Sciences
Open Access
Discussions

provide new ideas for simulation and early warning of floods. In addition, due to the governing equations od DRM is ordinary differential equations (ODEs), the computational efficiency of DRM is much higher than DW model, which governed by nonlinear partial differential equations (PDEs). More attention should be paid on the determination of the nonlinear relationship of the water storage ratio curve under different geographical scenarios, which will benefit to propose more efficient flood forecasting methods or early warning systems.

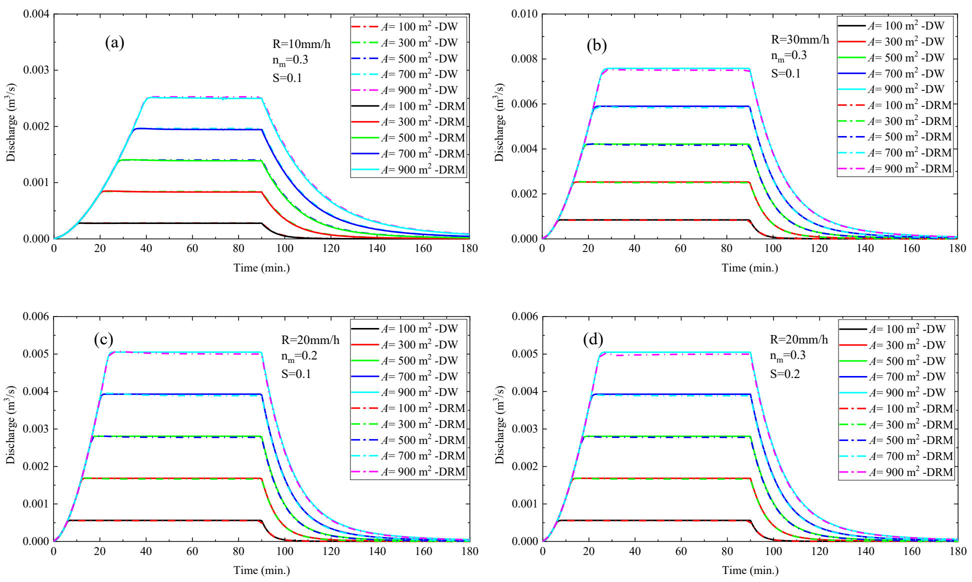

Fig. 4. Comparative analyses of discharge calculated by DW and DRM under designed rainfall. (a) controlled group; (b) compared with (a), only the rainfall intensity is changed; (c) compared with (a), rainfall intensity and Manning coefficient are changed; (d) compared with (a), rainfall intensity and slope gradient are changed.

5. Fluctuation of water storage ratio under natural rainfall conditions

After implementing a real rainfall event in the impermeable conceptual slope model (Fig. 1c), the change of the water storage ratio is calculated as shown in Fig. 5. Rainfall data was recorded from 09 August 2022 00:00 - 10 August 2022 00:00 in Aomori Prefecture, Japan (https://www.data.jma.go.jp). The total

https://doi.org/10.5194/hess-2024-25
Preprint. Discussion started: 5 March 2024
© Author(s) 2024. CC BY 4.0 License.
Hydrology and Earth System Sciences
Open Access
Discussions

simulation time is 30 hours. Results show that in addition to the fluctuations of water storage ratio in the beginning and end stages of rainfall, there are mainly five fluctuation periods of water storage ratio during the rainfall duration stage, i.e., 1#, 2#, 3#, 4#, and 5# fluctuation (Fig. 5). The fluctuations are found to be mainly caused by weak rainfall (R<5.0 mm h^{-1}) as pointed by the red arrows in Fig. 5.

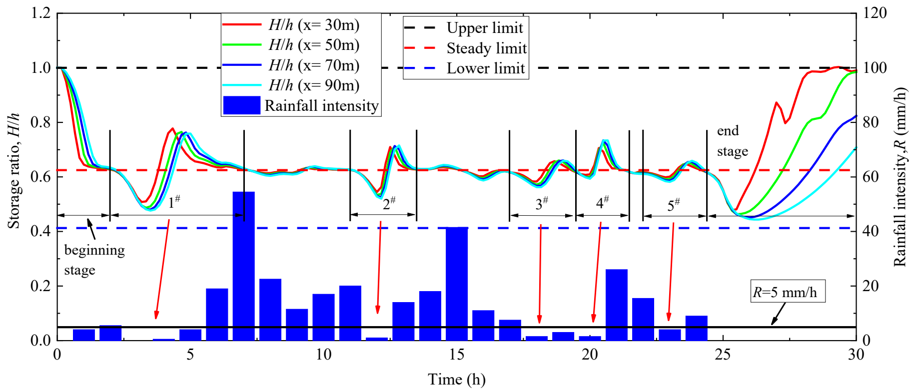

Fig. 5. The fluctuation of water storage ratio and the effectiveness of DRM in natural rainfall events.

Besides, the fluctuations of water storage ratio can be divided into three modes, that is Mode I during rainfall beginning stage (Fig. 6a), Mode II during rainfall duration stage (Fig. 6b), and Mode III during rainfall end stage (Fig. 6c). This means that the certainty of the fluctuation modes will provide the possibility for quantitative analysis of the fluctuation of the water storage ratio induced by the change of the rainfall intensity.

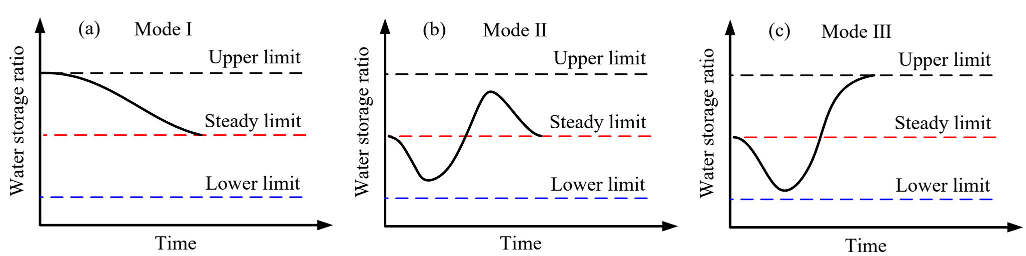

Fig. 6. Three kinds of water storage ratio fluctuation mode in natural rainfall events. (a) water storage ratio fluctuation Mode I during rainfall beginning stage; (b) water storage ratio fluctuation Mode II during rainfall duration stage; (c) water storage ratio fluctuation Mode III during rainfall end stage.

https://doi.org/10.5194/hess-2024-25
Preprint. Discussion started: 5 March 2024
© Author(s) 2024. CC BY 4.0 License.

Figure 7 shows the simulation results of discharge at different locations calculated by DRM and DW model. Results suggest that after the determination of the water storage ratio fluctuations, the calculation results of DRM are in good agreement with those of DW model, meaning that DRM provides a new and more effective theoretical scheme for flood prediction.

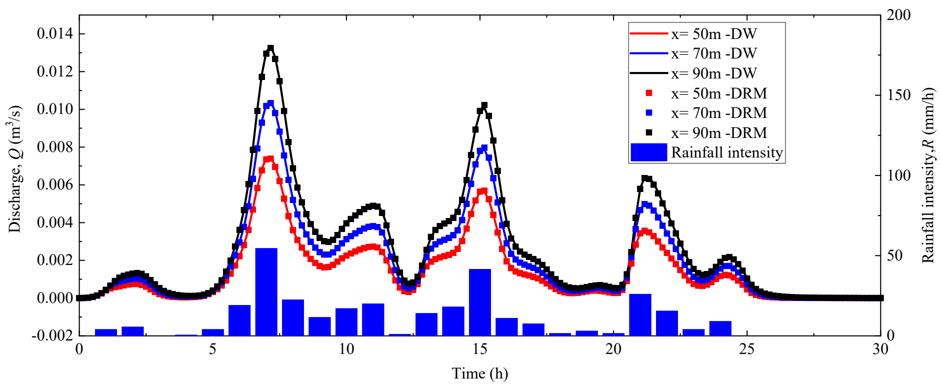

Fig. 7. Time-dependent discharge calculated by DRM and DW model.

6. Discussions and Conclusions

Through the numerical simulations of the hydrodynamic model, we find that in the rainfall-runoff process, three limits (upper, steady, and lower limit) control the water storage in a catchment, which are independent of meteorological (rainfall intensity), vegetation (Manning's coefficient), and terrain (slope gradient) conditions. The value of the three limits is approximately 1.0, 0.625, and 0.4125, respectively. Under the control of these three limits, a "plume" shaped nonlinear relationship exists between the inside average water depth and the outlet water depth in a catchment, namely the water storage ratio. Meteorological, vegetation, and terrain conditions only affect the size of the "plume" without changing its shape.

In addition, the water storage and discharge are limited to envelope lines and the discharge/water depth process lines during water rising and falling showed a grid-shaped distribution, which might be the cause of the looped rating curve, i.e., higher discharges for the rising limb than for the recession limb at the same

https://doi.org/10.5194/hess-2024-25
Preprint. Discussion started: 5 March 2024
© Author(s) 2024. CC BY 4.0 License.
Hydrology and Earth System Sciences
Discussions

stage. Rainfall, especially weak rain (rainfall intensity is less than 5.0 mm h^{-1}) significantly affects the fluctuations of water storage ratio, which can be divided into three modes, that is Mode I during rainfall beginning stage, Mode II during rainfall duration stage, and Mode III during rainfall end stage.

The findings in this study provide a key to establish a simpler prediction model for floods. Afterward, we constructed a hydrological-hydrodynamic integrated model, namely the Distributed Runoff Model (DRM). Based on a real rainfall event, numerical results indicate that DRM quickly reproduces the calculation results of the time-consuming hydrodynamic model, meaning that the determination of the nonlinear relationship of the water storage ratio curve under different geographical scenarios will provide new ideas for simulation and early warning of floods.

Authors' contributions

Yulong Zhu: Conceptualization, Methodology, Software, Validation, Formal Analysis, Investigation, Data Curation, Writing-Original draft, Writing - Review & Editing.

Yang Zhou: Methodology, Validation, Investigation, Resources, Data Curation.

Xiaorong Xu: Methodology, Investigation, Data Curation.

Changqing Meng: Validation, Investigation, Data Curation.

Yuankun Wang: Conceptualization, Methodology, Writing-Original draft, Writing - Review & Editing, Supervision, Project administration, Funding acquisition.

Availability of data and materials

The datasets used and/or analyzed during the current study are available from the corresponding author on reasonable request.

https://doi.org/10.5194/hess-2024-25
Preprint. Discussion started: 5 March 2024
© Author(s) 2024. CC BY 4.0 License.

Hydrology and Earth System Sciences
Discussions
Open Access
EGU

Competing interests

The authors declare that they have no conflict of interest.

Acknowledgments

This study was supported by National Natural Science Fund of China (52279064) and the Fundamental Research Funds for the Central Universities of China (2021MS043).

References

Abbott, M. B., Bathurst, J. C., Cunge, J. A., O'Connell, P. E., and Rasmussen, J.: An introduction to the European Hydrological System-Systeme Hydrologique Europeen,"SHE", 1: History and philosophy of a physically-based, distributed modelling system. Journal of Hydrology, 87(1-2), 45-59, https://doi.org/10.1016/0022-1694(86)90114-9, 1986.

Almazroui, M.: Rainfall trends and extremes in Saudi Arabia in recent decades. Atmosphere, 11(9), 964, https://doi.org/10.3390/atmos11090964, 2020.

Arnold, J. G., and Williams, J. R.: Validation of SWRRB: Simulator for water resources in rural basins. J. Water Resour. Plan. Manage. ASCE, 113(2), 243-256, https://doi.org/10.1061/(ASCE)0733-9496(1987)113:2(243), 1987.

Beven, K. J. and Kirkby, M. J.: A Physically Based Variable Contributing Area Model of Basin Hydrology. Hydrological Sciences Bulletin, 24, 43-69, https://doi.org/10.1080/02626667909491834, 1979.

Bevacqua, E., Vousdoukas, M. I., Zappa, G., Hodges, K., Shepherd, T. G., Maraun, D., Mentaschi, L., and Feyen, L.: More meteorological events that drive compound coastal flooding are projected under climate change. Communications Earth & Environment, 1(1), 47, https://doi.org/10.1038/s43247-020-00044-z, 2020.

https://doi.org/10.5194/hess-2024-25
Preprint. Discussion started: 5 March 2024
© Author(s) 2024. CC BY 4.0 License.

Cabré, A., Remy, D., Marc, O., Burrows, K., and Carretier, S.: Flash floods triggered by the 15-17th March 2022 rainstorm event in the Atacama Desert mapped from InSAR coherence time series. Natural Hazards, 116(1), 1345-1353, https://doi.org/10.1007/s11069-022-05707-y, 2023.

Cai, W., Borlace, S., Lengaigne, M., van Rensch, P., Collins, M., Vecchi, G., Timmermann, A., Santoso, A., McPhaden, M. J., Wu, L., England, M. H., Wang, G., Guilyardi, E., and Jin, F. F.: Increasing frequency of extreme El Niño events due to greenhouse warming. Nature Climate Change, 4(2), 111-116, https://doi.org/10.1038/nclimate2100, 2014.

Camassa, R., Holm, D. D., and Hyman, J. M.: A new integrable shallow water equation. Advances in Applied Mechanics, 31, 1-33, https://doi.org/10.1016/S0065-2156(08)70254-0, 1994.

Crawford, N. H. and Linsley, R. K.: Digital Simulation in Hydrology: Stanford Watershed Model IV. Technical Report No. 39, Department of Civil Engineering, Stanford University, pp. 210, 1966.

Crossley, A., Lamb, R., Waller, S., and Dunning, P.: Fast 2D flood modelling using GPU technology-recent applications and new developments. In EGU General Assembly Conference Abstracts, p. 12043, 2010.

Hoch, J. M., Eilander, D., Ikeuchi, H., Baart, F., and Winsemius, H. C.: Evaluating the impact of model complexity on flood wave propagation and inundation extent with a hydrologic–hydrodynamic model coupling framework. Natural Hazards and Earth System Sciences, 19(8), 1723-1735, https://doi.org/10.5194/nhess-19-1723-2019, 2019.

Hsu, P. C., Xie, J., Lee, J. Y., Zhu, Z., Li, Y., Chen, B., and Zhang, S.: Multiscale interactions driving the devastating floods in Henan Province, China during July 2021. Weather and Climate Extremes, 39, 100541, https://doi.org/10.1016/j.wace.2022.100541, 2023.

Kim, J., Warnock, A., Ivanov, V. Y., and Katopodes, N. D.: Coupled modeling of hydrologic and hydrodynamic processes including overland and channel flow. Advances in Water Resources, 37, 104-126, https://doi.org/10.1016/j.advwatres.2011.11.009, 2012.

© Author(s) 2024. CC BY 4.0 License.

Kirezci, E., Young, I. R., Ranasinghe, R., Muis, S., Nicholls, R. J., Lincke, D., and Hinkel, J.: Projections of global-scale extreme sea levels and resulting episodic coastal flooding over the 21st Century. Scientific Reports, 10(1), 11629, https://doi.org/10.1038/s41598-020-67736-6, 2020.

Kobayashi, K., Duc, L., Kawabata, T., Tamura, A., Oizumi, T., Saito, K., Nohara, D., and Sumi, T.: Ensemble rainfall–runoff and inundation simulations using 100 and 1000 member rainfalls by 4D LETKF on the Kumagawa River flooding 2020. Progress in Earth and Planetary Science, 10(1), 1-22, https://doi.org/10.1186/s40645-023-00537-3, 2023.

Köhne, J. M., Wöhling, T., Pot, V., Benoit, P., Leguédois, S., Le Bissonnais, Y., and Šimůnek, J.: Coupled simulation of surface runoff and soil water flow using multi-objective parameter estimation. Journal of Hydrology, 403(1-2), 141-156, https://doi.org/10.1016/j.jhydrol.2011.04.001, 2011.

Lee, J., Perera, D., Glickman, T., and Taing, L. Water-related disasters and their health impacts: A global review. Progress in Disaster Science, 8, 100123, https://doi.org/10.1016/j.pdisas.2020.100123, 2020.

Li, M., and Yao, J.: Precipitation extremes observed over and around the Taklimakan Desert, China. PeerJ, 11, e15256, https://doi.org/10.7717/peerj.15256, 2023.

Li, P. W., and Fan, C. M.: Generalized finite difference method for two-dimensional shallow water equations. Engineering Analysis with Boundary Elements, 80, 58-71, https://doi.org/10.1016/j.enganabound.2017.03.012, 2017.

Liu, Z., Zhang, H., and Liang, Q.: A coupled hydrological and hydrodynamic model for flood simulation. Hydrology Research, 50(2), 589-606, https://doi.org/10.2166/nh.2018.090, 2019.

Merkuryeva, G., Merkuryev, Y., Sokolov, B. V., Potryasaev, S., Zelentsov, V. A., and Lektauers, A.: Advanced river flood monitoring, modelling and forecasting. Journal of Computational Science, 10, 77-85, https://doi.org/10.1016/j.jocs.2014.10.004, 2015.

Merz, B., Blöschl, G., Vorogushyn, S., Dottori, F., Aerts, J. C., Bates, P., Bertola, M., Kemter, M., Kreibich, H., Lall, U., and Macdonald, E.: Causes, impacts and patterns of disastrous river floods. Nature Reviews Earth & Environment, 2(9), 592-609, https://doi.org/10.1038/s43017-021-00195-3, 2021.

Ming, X., Liang, Q., Xia, X., Li, D., and Fowler, H. J.: Real-time flood forecasting based on a high-performance 2-D hydrodynamic model and numerical weather predictions. Water Resources Research, 56(7), e2019WR025583, https://doi.org/10.1029/2019WR025583, 2020.

Mori, K., Tada, K., Tawara, Y., Ohno, K., Asami, M., Kosaka, K., and Tosaka, H.: Integrated watershed modeling for simulation of spatiotemporal redistribution of post-fallout radionuclides: application in radiocesium fate and transport processes derived from the Fukushima accidents. Environmental Modelling & Software, 72, 126-146, https://doi.org/10.1016/j.envsoft.2015.06.012, 2015.

Najibi, N., and Devineni, N.: Recent trends in the frequency and duration of global floods. Earth System Dynamics, 9(2), 757-783, https://doi.org/10.5194/esd-9-757-2018, 2018.

Nanditha, J. S., Kushwaha, A. P., Singh, R., Malik, I., Solanki, H., Chuphal, D. S., Dangar, S., Mahto, S. S., Vegad, U., and Mishra, V.: The Pakistan flood of August 2022: Causes and implications. Earth's Future, 11(3), e2022EF003230, https://doi.org/10.1029/2022EF003230, 2023.

Petersen-Øverleir, A.: Modelling looped rating curves. In Proc., XXIV Nordic Hydrological Conf, pp. 139-146, https://doi.org/10.13140/2.1.1069.4403, 2006.

Ruidas, D., Saha, A., Islam, A. R. M. T., Costache, R., and Pal, S. C.: Development of geo-environmental factors controlled flash flood hazard map for emergency relief operation in complex hydro-geomorphic environment of tropical river, India. Environmental Science and Pollution Research, 30, 106951-106966, https://doi.org/10.1007/s11356-022-23441-7, 2022.

Sanders, B. F., Schubert, J. E., and Detwiler, R. L.: ParBreZo: A parallel, unstructured grid, Godunov-type, shallow-water code for high-resolution flood inundation modeling at the regional scale. Advances in Water Resources, 33(12), 1456-1467, https://doi.org/10.1016/j.advwatres.2010.07.007, 2010.

© Author(s) 2024. CC BY 4.0 License.

Sugawara, M.: The development of hydrological model-tank. Time and the River: essays by eminent hydrologists., 201-258, 1995.

Tellman, B., Sullivan, J.A., Kuhn, C., Kettner, A. J., Doyle, C. S., Brakenridge, G. R., Erickson, T. A., and Slayback, D. A.: Satellite imaging reveals increased proportion of population exposed to floods. Nature, 596, 80-86, https://doi.org/10.1038/s41586-021-03695-w, 2021.

Tradowsky, J. S., Philip, S. Y., Kreienkamp, F., Kew, S. F., Lorenz, P., Arrighi, J., ... and Wanders, N.: Attribution of the heavy rainfall events leading to severe flooding in Western Europe during July 2021. Climatic Change, 176(7), 90, https://doi.org/10.1007/s10584-023-03502-7, 2023.

Valente, M., Zanellati, M., Facci, G., Zanna, N., Petrone, E., Moretti, E., Barone-Adesi, F., and Ragazzoni, L.: Health system response to the 2023 floods in Emilia-Romagna, Italy: a field report. Prehospital and Disaster Medicine, 38(6), 813-817, https://doi.org/10.1017/S1049023X23006404, 2023.

Ward, P. J., Jongman, B., Kummu, M., Dettinger, M. D., Sperna Weiland, F. C., and Winsemius, H. C.: Strong influence of El Niño Southern Oscillation on flood risk around the world. Proceedings of the National Academy of Sciences, 111(44), 15659-15664, https://doi.org/10.1073/pnas.1409822111, 2014.

Wu, H., Chen, B., Ye, X. et al.: An improved calibration and uncertainty analysis approach using a multicriteria sequential algorithm for hydrological modeling. Scientific Reports, 11, 16954, https://doi.org/10.1038/s41598-021-96250-6, 2021.

Zhu, Y. L., Ishikawa, T., Subramanian, S.S., and Luo, B.: Simultaneous analysis of slope instabilities on a small catchment-scale using coupled surface and subsurface flows. Engineering Geology, 275, 105750, https://doi.org/10.1016/j.enggeo.2020.105750, 2020.

Zhu, Y. L., Zhang, Y. F., Yang, J., Nguyen, B. T., and Wang, Y.: A novel method for calculating distributed water depth and flow velocity of stormwater runoff during the heavy rainfall events. Journal of Hydrology, 612, 128064, https://doi.org/10.1016/j.jhydrol.2022.128064, 2022.